Generation of Optical Vortex Array by the Quasi-Talbot Effect With All-Dielectric Metasurface

Guangzhou Geng, Zhancheng Li, Wei Zhu, Ruhao Pan, Wenwei Liu, Hua Cheng, Wenyuan Zhou, Junjie Li, Jianguo Tian, and Shuqi Chen

***Abstract*— In this letter, we numerically and experimentally demonstrate the highly efficient generation of optical vortex arrays based on the quasi-Talbot effect with a reflective all-dielectric metasurface, which is composed of six identical orbital angular momentum lenses. Six separated and focused optical vortices at the focal plane can be high efficiently generated, and form a vortex array at the defocusing plane through the quasi-Talbot effect. The proposed metasurface is made from a commercial silicon on insulator wafer with a high integrated level, which enables the integration of our approach in on-chip platforms for optical lithography and manipulation applications.**

***Index Terms*— All-dielectric metasurface, optical vortex array, quasi-Talbot effect, silicon on insulator wafer (SOI).**

I. Introduction

OPTICAL waves carrying orbital angular momentum (OAM) are named vortex beams, and they have doughnut-shaped transverse intensity profiles with hollow intensity distributions and helical phase maps. Optical vortex beams have drawn widespread interest from the scientific community in the last thirty years since they show unprecedented capacities in applications such as free space communication [1], super-resolution microscopy [2], [3], quantum information processing [4], [5] and optical tweezer [6], [7], [8]. Optical vortex beams have been widely generated and modulated by conventional spiral phase plates [9], [10] and fork diffraction gratings [11], [12]. In addition to optical vortex beams, optical vortex arrays composed of periodically arranged optical vortex beams have recently received increasing attention. Compared with isolated optical vortex beams, optical vortex arrays show some distinct advantages in trapping and manipulation-based applications [13], [14], [15], [16]. As a result, various methods have been proposed to generate optical vortex arrays, including multi-beam interference [17], [18], specially designed diffraction gratings [19], [20], and optical multiplexing based on sub-wavelength phase manipulation [21], [22], [23].

Recent advances have demonstrated that the Talbot effect is a good candidate for generating optical vortex arrays. The Talbot effect is a self-imaging effect, which is described as the appearance of the imitative image of a periodic structure at periodic distances behind the structure under plane wave illumination [24], [25]. The quasi-Talbot effect has a larger multiplication factor and is caused by optical wave interference from aperiodic structures, whose centers are placed in a rotationally symmetric position. Recently, the quasi-Talbot effect has been utilized in the design of plasmonic metasurfaces to realize optical vortex arrays [26]. However, its efficiency is approximately 1% due to ohmic loss. Compared with plasmonic metasurfaces composed of metallic nanostructures, all-dielectric metasurfaces can more efficiently manipulate optical waves since their ohmic loss is negligible. Meanwhile, all-dielectric metasurfaces prefer to be fabricated on commercial silicon-on-insulator (SOI) wafers used in mass semiconductor production, which will make the fabrication of metasurfaces more effective and compatible, benefiting their application and integration in on-chip platforms. An all-dielectric metasurface fabricated on a commercial SOI wafer for highly efficient optical vortex array generation based on the quasi-Talbot effect has yet to be presented.

In this letter, we propose highly efficient all-dielectric metasurfaces fabricated on a SOI wafer to realize optical vortex arrays. The metasurfaces are designed based on the quasi-Talbot effect and consist of six identical OAM lenses tangent to each other. The phase profile of every OAM lens is designed

Manuscript received 11 December 2022; revised 21 February 2023; accepted 4 March 2023. Date of publication 8 March 2023; date of current version 16 March 2023. This work was supported in part by the National Key Research and Development Program of China under Grant 2021YFA1400601 and Grant 2022YFA1404501; in part by the National Natural Science Fund for Distinguished Young Scholars under Grant 11925403; in part by the National Natural Science Foundation of China under Grant 12122406, Grant 12192253, Grant 11974193, Grant 12274237, Grant 12274239, Grant 12074420, and Grant U22A20258; and in part by the 111 Project under Grant B23045. *(Corresponding author: Shuqi Chen.)*

Guangzhou Geng, Zhancheng Li, Wenwei Liu, Hua Cheng, Wenyuan Zhou, and Jianguo Tian are with the Key Laboratory of Weak Light Nonlinear Photonics, Ministry of Education, Smart Sensing Interdisciplinary Science Center, Renewable Energy Conversion and Storage Center, School of Physics, and the TEDA Institute of Applied Physics, Nankai University, Tianjin 300071, China (e-mail: zcli@nankai.edu.cn; hcheng@nankai.edu.cn; jjtian@nankai.edu.cn).

Wei Zhu, Ruhao Pan, and Junjie Li are with the Beijing National Laboratory for Condensed Matter Physics, Institute of Physics, Chinese Academy of Sciences, Beijing 100190, China (e-mail: jjli@iphy.ac.cn).

Shuqi Chen is with the Key Laboratory of Weak Light Nonlinear Photonics, Ministry of Education, Smart Sensing Interdisciplinary Science Center, Renewable Energy Conversion and Storage Center, School of Physics, and the TEDA Institute of Applied Physics, Nankai University, Tianjin 300071, China, and also with the Collaborative Innovation Center of Extreme Optics, Shanxi University, Taiyuan, Shanxi 030006, China (e-mail: schen@nankai.edu.cn).

Color versions of one or more figures in this letter are available at https://doi.org/10.1109/LPT.2023.3253869.

Digital Object Identifier 10.1109/LPT.2023.3253869

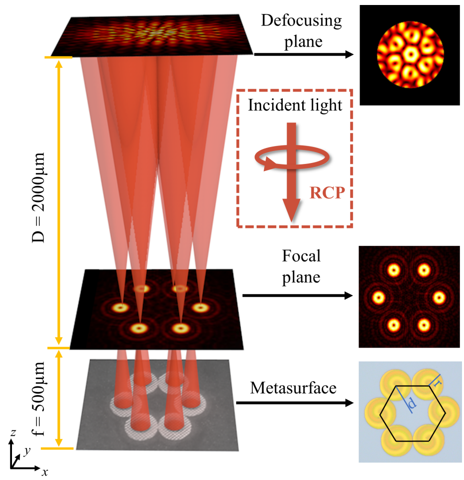

Fig. 1. Schematic of the designed reflective all-dielectric metasurface for optical vortex array generation.

by combining the spherical phase profile of a focal lens and the helical phase profile of a vortex beam. A crystalline silicon nanofin with high reflectance and high circular polarization conversion efficiency is demonstrated and used as the basic unit cell to constitute the OAM lens. The required phase profiles are fulfilled by utilizing the geometric phase and adjusting the orientation angles of the nanofins. The OAM lenses with topological charge $l = 1$ can generate focused optical vortices at the focal plane, and the focused optical vortices change into an optical vortex array on the defocusing plane due to the quasi-Talbot effect. The experimental results are in good agreement with the simulated results, validating the effectiveness of our approach. Our design provides a simple and promising candidate for further application of optical vortex arrays in optical lithography and manipulation.

II. Metasurface Design

The working principle of the designed metasurface is illustrated in Fig. 1. The designed metasurface is composed of six identical OAM lenses tangent to each other. The number of lenses has been optimized to get vortex beam arrays in dense gapless arrangement and good shape of vortex arrays. The centers of the OAM lenses are placed at the vertex positions of a regular hexagon. The radius of the circumcircle of this regular hexagon and the radius of the OAM lenses are set as $d = 34$ μm and $r = 17$ μm, respectively. For 633 nm right-handed circularly polarized (RCP) plane waves illuminating along the -z direction, each OAM lens can reflect the incident waves with high efficiency, changing their spins and generating a focused optical vortex at the focal plane. As a result, six separate and focused vortices can be generated. The focused vortices will extend along the z-axis and interfere with each other on the defocusing plane, resulting in an optical vortex array through the quasi-Talbot effect. The generated optical vortex array is attributed to the quasi-Talbot effect instead of the Talbot effect since the focused optical vortices do not form a periodic structure. In our design, the focus length f of all OAM lenses is set as 500 μm, and the distance between the focal plane and the defocusing plane D is set as 2000 μm.

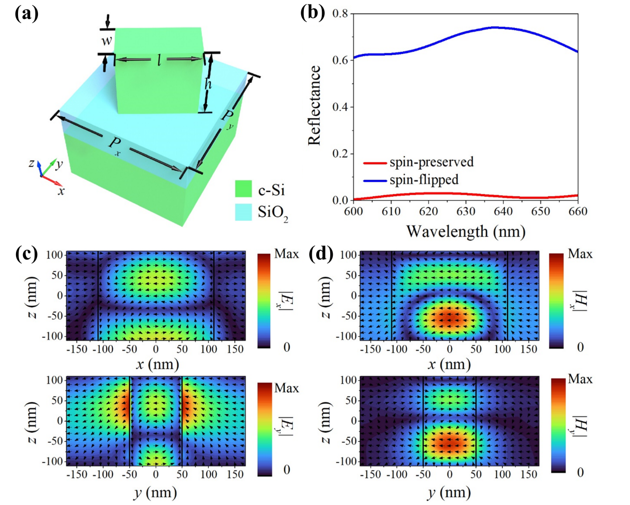

Fig. 2. (a) Schematic of the structural parameters of the nanofin. (b) Simulated reflectance of spin-preserved and spin-flipped waves under circularly polarized illumination. Simulated results of the field flows (black arrows) and amplitude distribution of the x- and y-components of the (c) electric field and the (d) magnetic field in the x-z ($y = 0$ nm) and y-z planes ($x = 0$ nm) under circularly polarized illumination at 633 nm.

The designed metasurface was fabricated on a commercial SOI substrate (widespread in the modern semiconductor industry) with a layer of 220 nm crystalline silicon (c-Si) separated from the bulk silicon substrate by a thin layer of 2 μm SiO_2. A nanofin was designed and optimized by using finite differential time domain method to constitute OAM lenses. The structural parameters of the nanofin are illustrated in Fig. 2(a). The periods in both the x and y directions are $P_x = P_y = 340$ nm, and the width w, length l, and height h of the nanofins are equal to 100 nm, 220 nm, and 220 nm, respectively. The height (h) of the nanofins is the same as the thickness of the top crystalline silicon layer of the commercial SOI substrate, and underneath SiO_2 acts as the etch stop layer to ensure height accuracy, reducing the etching difficulty. The nanofins can be regarded as near-perfect half-wave plates that can efficiently convert the spin state of incident circularly polarized waves into the opposite state, as shown in Fig. 2(b). By rotating the nanofins θ degrees along the z-axis, a phase delay of $\pm 2\theta$ due to the geometric phase can be added to left-handed and right-handed polarized reflection waves, respectively. As a result, the designed nanofins can be used to manipulate the phase of reflection waves with over 60% efficiency from 600 to 660 nm, ensuring the high efficiency of the six OAM lenses. The nanofin with C_{2z} rotational symmetry can be treated as an anisotropic optical resonator, which can reflect x- and y-polarized incident waves with similar efficiency, and the phase difference between the reflected x- and y-polarized waves is close to π, resulting in the circularly polarization conversion with high efficiency. The anisotropic optical response of the designed nanofins can be attributed to the simultaneous excitation of electric and magnetic resonances. To validate the results, we simulated the flows and distributions of the electric and magnetic fields in the x-z and y-z planes under circularly polarized illumination at 633 nm, as shown in Figs. 2(c) and 2(d). Both the x- and y-components of the electric and magnetic fields are localized and enhanced

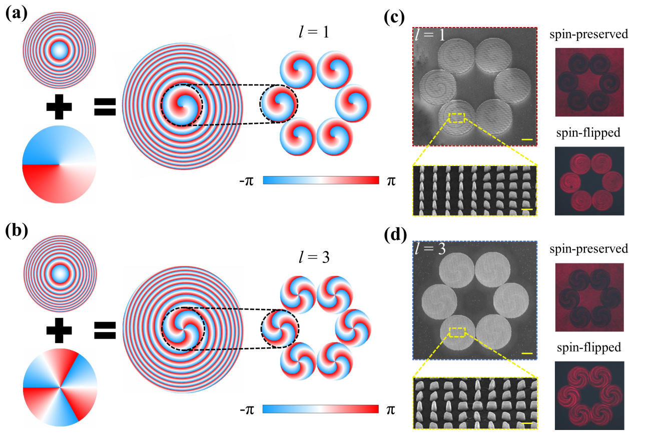

Fig. 3. The phase profile of the two designed metasurfaces for generating optical vortex arrays with topological charge (a) $l = 1$ and (b) $l = 3$. SEM images of the fabricated metasurfaces for the realization of optical vortex arrays with (c) $l = 1$ and (d) $l = 3$, and their optical images captured under different polarization detection conditions. The scale bars of the total and enlarged SEM images are 10 μm and 300 nm, respectively.

inside the nanofin, verifying the existence of electric and magnetic resonances in both the x and y directions.

The OAM lenses consist of nanofins with different orientation angles to fulfil the required phase profile ϕ obtained by combining the spherical phase profile ϕ_s of a focal lens and the helical phase profile ϕ_h of a vortex beam:

$$\phi = \phi_s + \phi_h. \tag{1}$$

Figs. 3(a) and 3(b) illustrate the phase profile of the designed OAM lens with topological charges $l = 1$ and $l = 3$, respectively, which are linear additions of a spherical phase profile and a helical phase profile. As a result, the phase delay of every nanofin in the OAM lens can be expressed as:

$$\varphi(x, y) = -\frac{2\pi}{\lambda}(\sqrt{x^2 + y^2 + f^2} - f) + l \times \arctan(\frac{y}{x}). \tag{2}$$

where f is the focal length of the OAM lens and l is the topological charge of the reflected vortex beam. The scanning electron microscopy (SEM) images of the fabricated metasurfaces for the realization of optical vortex arrays with $l = 1$ and $l = 3$ are shown in Figs. 3(c) and 3(d). The enlarged SEM images of the metasurfaces reveal the good fidelity of the nanofins.

III. Results and Discussion

We captured the optical images of the fabricated samples for the realization of optical vortex arrays with $l = 1$ and $l = 3$ under different polarization detection conditions at 633 nm, as presented in Figs. 3(c) and 3(d). The spin-preserved component of reflection waves from the OAM lenses is negligible since the OAM lenses in the two samples are dark while the substrate is bright. In contrast, the spin-flipped component of reflection waves from the OAM lenses is significant since the OAM lenses are bright while the substrate is dark. The captured images of the fabricated samples validate that the nanofins have high reflectance and high circular polarization conversion efficiency.

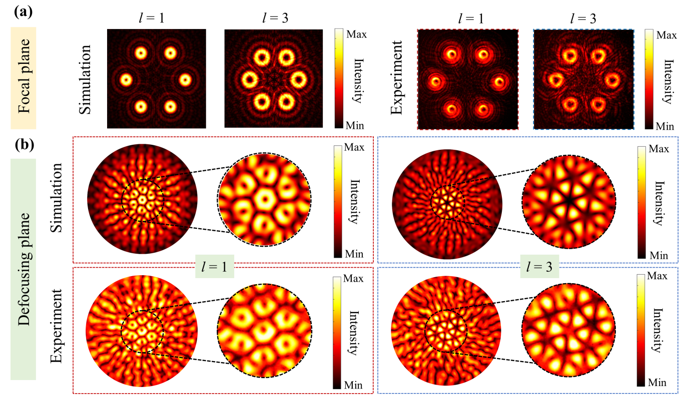

Fig. 4. Numerical and experimental validation of the optical vortex arrays generated by the designed metasurfaces. (a) Simulated (left) and experimental (right) results of vortex beam spots with topological charges equal to 1 and 3 on the focal plane. (b) Simulated (top) and experimental (bottom) results of generated vortex arrays (left: $l = 1$, right: $l = 3$) on the defocusing plane.

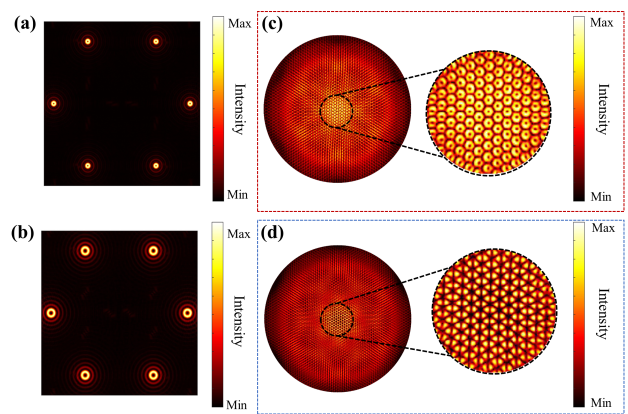

Fig. 5. Increasing the number of vortices by change the distance between the OAM lenses from $d = 34$ μm to $d = 170$ μm. Simulated vortex beam spots on the focal plane for the two designed metasurfaces with topological charge (a) $l = 1$ and (b) $l = 3$. Generated vortex arrays on the defocusing plane for the two designed metasurfaces with topological charge (c) $l = 1$ and (d) $l = 3$.

We further simulated and measured the optical field distributions on the focal and defocusing planes, as shown in Fig. 4. The simulated results were conducted using vector diffraction integral method. For the two designed metasurfaces, six separate and identical focused vortices can be observed at the focal plane, as shown in Fig. 4(a). The simulated and measured results are in good agreement. A charge-dependent increase in the vortex core can be observed for focused vortices with $l = 3$. The optical field extends along the z-axis and interfere with each other on the defocusing plane, generating optical vortex arrays on the defocusing plane due to the quasi-Talbot effect. Fig. 4(b) shows the simulated and measured field distributions on the defocusing plane for metasurfaces with $l = 1$ and $l = 3$. The agreement between the numerical and measured results demonstrates the precise fabrication of our metasurfaces.

Despite the good agreement between the simulated and measured results, an optical vortex array can be observed for the metasurface with $l = 1$, while an optical vortex array with interference pattern instead of an optical vortex array can be observed on the defocusing plane for the metasurface with $l = 3$. Owing to the larger vortex core for an optical vortex with $l = 3$, both the number of OAM lenses and the observation distance need to be increased to observe the optical vortex array [27]. Meanwhile, since the six OAM lenses are tangent to each other, the optical vortex arrays are only in a small center area on the defocusing plane. Optical vortex arrays with a greater number of vortices can be obtained by increasing the distance between the OAM lenses or the radius of the OAM lenses. For example, if we change the distance between the OAM lenses in the two designed metasurfaces with $l = 1$ and $l = 3$ from $d = 34$ μm into $d = 170$ μm (the distance between the focal plane and the defocusing plane increases to 8000 μm accordingly), the number of vortices can significantly increase, as validated by the results in Fig. 5.

IV. Conclusion

In summary, we numerically and experimentally demonstrated that all-dielectric metasurfaces fabricated on a commercial SOI wafer can be used to efficiently generate optical vortex arrays based on the quasi-Talbot effect. We designed and optimized a crystalline silicon nanofin to reach high reflectance and high circular polarization conversion efficiency from 600 to 660 nm. The designed nanofin is then used as the basic unit cell to constitute the six identical OAM lenses of each metasurface. With both simulated and experimental validation, we proved that the six OAM lenses with $l = 1$ can generate six separated and focused optical vortices at the focal plane, and the focused vortices will extend along the z-axis and change into a vortex array at the defocusing plane through the quasi-Talbot effect. The number of vortices in a generated optical vortex array for a metasurface with $l = 1$ can be further increased by adjusting the distance between the OAM lenses. Our designs demonstrate that highly efficient optical vortex arrays can be effectively generated with all-dielectric metasurfaces fabricated on the SOI wafer, providing fertile ground for further application of optical vortex arrays in optical lithography and manipulation.

References

[1] H.-L. Zhou et al., "Orbital angular momentum complex spectrum analyzer for vortex light based on the rotational Doppler effect," *Light, Sci. Appl.*, vol. 6, no. 4, Nov. 2016, Art. no. e16251.

[2] W. Yu et al., "Super-resolution deep imaging with hollow Bessel beam STED microscopy," *Laser Photon. Rev.*, vol. 10, no. 1, pp. 147–152, Jan. 2016.

[3] Z. Zhao et al., "Multispectral optical metasurfaces enabled by achromatic phase transition," *Sci. Rep.*, vol. 5, no. 1, p. 15781, Oct. 2015.

[4] X.-B. Song et al., "Experimental observation of quantum Talbot effects," *Phys. Rev. Lett.*, vol. 107, no. 3, Jul. 2011, Art. no. 033902.

[5] H. Jin, P. Xu, J. S. Zhao, H. Y. Leng, M. L. Zhong, and S. N. Zhu, "Observation of quantum Talbot effect from a domain-engineered nonlinear photonic crystal," *Appl. Phys. Lett.*, vol. 101, no. 21, Nov. 2012, Art. no. 211115.

[6] D. G. Grier, "A revolution in optical manipulation," *Nature*, vol. 424, no. 6950, pp. 810–816, Aug. 2003.

[7] W. P. Wang et al., "Hollow plasma acceleration driven by a relativistic reflected hollow laser," *Phys. Rev. Lett.*, vol. 125, no. 3, Jul. 2020, Art. no. 034801.

[8] Y. Tian, L. Wang, G. Duan, and L. Yu, "Multi-trap optical tweezers based on composite vortex beams," *Opt. Commun.*, vol. 485, Apr. 2021, Art. no. 126712.

[9] M. W. Beijersbergen, R. P. C. Coerwinkel, M. Kristensen, and J. P. Woerdman, "Helical-wavefront laser beams produced with a spiral phaseplate," *Opt. Commun.*, vol. 112, pp. 321–327, Dec. 1994.

[10] J. Zhou and P. T. Lin, "Generation of mid-infrared vortex beams by 3-D printed polymer phase plates," *Opt. Laser Technol.*, vol. 156, Dec. 2022, Art. no. 108509.

[11] S. Chen, Y. Cai, G. Li, S. Zhang, and K. W. Cheah, "Geometric metasurface fork gratings for vortex-beam generation and manipulation," *Laser Photon. Rev.*, vol. 10, no. 2, pp. 322–326, Mar. 2016.

[12] L. Yanming, K. Jihwan, and J. E. Michael, "Controlling orbital angular momentum using forked polarization gratings," *Proc. SPIE*, vol. 7789, pp. 118–129, Aug. 2010.

[13] K. Ladavac and D. G. Grier, "Microoptomechanical pumps assembled and driven by holographic optical vortex arrays," *Opt. Exp.*, vol. 12, no. 6, pp. 1144–1149, 2004.

[14] Z. Long, H. Hu, X. Ma, Y. Tai, and X. Li, "Encoding and decoding communications based on perfect vector optical vortex arrays," *J. Phys. D, Appl. Phys.*, vol. 55, no. 43, Oct. 2022, Art. no. 435105.

[15] Z. Shang, S. Fu, L. Hai, Z. Zhang, L. Li, and C. Gao, "Multiplexed vortex state array toward high-dimensional data multicasting," *Opt. Exp.*, vol. 30, no. 19, pp. 34053–34063, 2022.

[16] L. Zhu, A. Wang, M. Deng, B. Lu, and X. Guo, "Experimental demonstration of multiple dimensional coding decoding for image transfer with controllable vortex arrays," *Sci. Rep.*, vol. 11, no. 1, p. 12012, Jun. 2021.

[17] H. Fan et al., "Flower-shaped optical vortex array," *Annalen Physik*, vol. 533, no. 4, Apr. 2021, Art. no. 2000575.

[18] H. Zhang et al., "Grafted optical vortex with controllable orbital angular momentum distribution," *Opt. Exp.*, vol. 27, no. 16, pp. 22930–22938, 2019.

[19] N. Zhang, X. C. Yuan, and R. E. Burge, "Extending the detection range of optical vortices by Dammann vortex gratings," *Opt. Lett.*, vol. 35, no. 20, pp. 3495–3497, 2010.

[20] H. Wang, S. Fu, and C. Gao, "Tailoring a complex perfect optical vortex array with multiple selective degrees of freedom," *Opt. Exp.*, vol. 29, no. 7, pp. 10811–10824, 2021.

[21] L. Huang et al., "Volumetric generation of optical vortices with metasurfaces," *ACS Photon.*, vol. 4, no. 2, pp. 338–346, 2017.

[22] Z. H. Jiang, L. Kang, W. Hong, and D. H. Werner, "Highly efficient broadband multiplexed millimeter-wave vortices from metasurface-enabled transmit-arrays of subwavelength thickness," *Phys. Rev. A, Gen. Phys.*, vol. 9, no. 6, Jun. 2018, Art. no. 064009.

[23] F. Yue et al., "Multichannel polarization-controllable superpositions of orbital angular momentum states," *Adv. Mater.*, vol. 29, no. 15, Apr. 2017, Art. no. 1603838.

[24] L. Rayleigh, "On copying diffraction-gratings, and on some phenomena connected therewith," *Philos. Mag. J. Sci.*, vol. 11, no. 67, pp. 196–205, 1881.

[25] J. Wen, Y. Zhang, and M. Xiao, "The Talbot effect: Recent advances in classical optics, nonlinear optics, and quantum optics," *Adv. Opt. Photon.*, vol. 5, no. 1, pp. 83–130, Mar. 2013.

[26] H. Gao et al., "Quasi-talbot effect of orbital angular momentum beams for generation of optical vortex arrays by multiplexing metasurface design," *Nanoscale*, vol. 10, no. 2, pp. 666–671, 2018.

[27] M. Piccardo, M. de Oliveira, A. Toma, V. Aglieri, A. Forbes, and A. Ambrosio, "Vortex laser arrays with topological charge control and self-healing of defects," *Nature Photon.*, vol. 16, no. 5, pp. 359–365, May 2022.